Ezrin, Radixin, and Moesin Are Phosphorylated in Response to 2-Methoxyestradiol and Modulate Endothelial Hyperpermeability

Natalia V. Bogatcheva[1], Marina A. Zemskova[1], Boris A. Gorshkov[1], Kyung Mi Kim[1], Gregory A. Daglis[1], Christophe Poirier[1], and Alexander D. Verin[1]

[1]Vascular Biology Center, Georgia Health Sciences University, Augusta, Georgia

We showed previously that microtubule disruptor 2-methoxyestradiol (2ME) induces hyperpermeability of the endothelial monolayer via mechanisms that include the activation of p38 and Rho kinase (ROCK) and rearrangement of the actin cytoskeleton. Using the protein kinase C (PKC) inhibitors Ro-31–7549 and Ro-32–0432, we show *in vitro* and *in vivo* that 2ME-induced barrier dysfunction is also PKC-dependent. The known PKC substrates ezrin, radixin, and moesin (ERM) were recently implicated in the regulation of endothelial permeability. This study tested the hypotheses that ERM proteins are phosphorylated in response to 2ME, and that this phosphorylation is involved in 2ME-induced barrier dysfunction. We show that the application of 2ME leads to a dramatic increase in the level of ERM phosphorylation. This increase is attenuated in cells pretreated with the microtubule stabilizer taxol. In human pulmonary artery endothelial cells (HPAECs), the phosphorylation of ERM occurs in a p38-dependent and PKC-dependent manner. The activation of p38 appears to occur upstream from the activation of PKC, in response to 2ME. Phosphorylated ERM are localized at the cell periphery during the early phase of response to 2ME (15 minutes), and colocalize with F-actin branching points during the later phase of response (60 minutes). Using the short interfering RNA approach, we also showed that individual ERM depletion significantly attenuates 2ME-induced hyperpermeability. HPAEC monolayers, depleted of ERM proteins and monolayers, overexpressing phosphorylation-deficient ERM mutants, exhibit less attenuation of 2ME-induced barrier disruption in response to the PKC inhibitor Ro-31–7549. These results suggest a critical role of PKC activation in response to microtubule-disrupting agents, and implicate the phosphorylation of ERM in the barrier dysfunction induced by 2ME.

Keywords: 2-methoxyestradiol; ERM; PKC; phosphorylation; barrier dysfunction

CLINICAL RELEVANCE

Clinical studies testing the anticancer efficacy of novel agent 2-methoxyestradiol (2ME) reported toxicities associated with vascular leakage and respiratory problems. We studied mechanisms linking 2ME-induced microtubule disruption to the activation of signaling pathways leading to endothelial hyperpermeability. We found that the activation of protein kinase C and the subsequent phosphorylation of ERM comprise the processes contributing to 2ME-induced vascular barrier dysfunction.

2-methoxyestradiol (2ME) is a natural derivative of estradiol metabolism, which exhibits antiproliferative and antiangiogenic properties when used at pharmacological concentrations (1). 2ME is currently undergoing clinical trials to establish its efficacy as an anticancer drug, and to reveal its potential toxicities. One major problem encountered so far involves the low bioavailability of the orally delivered drug (2–5), which prompted the use of the nanodispersed 2ME form in trials (6, 7), and also instigated a search for 2ME analogues with better availability and a lower rate of degradation (8–11). At the same time, several studies using 2ME solo or in combination with other agents reported vascular-related side effects such as edema, angioedema, and dyspnea (2–6). These data reveal the multifaceted nature of the responses evoked by the anticancer agent 2ME. An elucidation of the signaling pathways leading to 2ME-induced vascular barrier dysfunction will help manage the unwanted side effects of 2ME, and ensure the safe clinical use of this promising anticancer compound.

Unlike receptor-interacting estradiol, 2ME elicits its effects by binding directly to microtubules (MTs) (12). Similar to colchicine, 2ME affects the process of MT polymerization. In endothelial cells, MT-disruptive compounds are known to induce a complex signaling response, leading to compromise of the endothelial barrier (13–15). Previously we reported that 2ME causes barrier dysfunction in HPAEC monolayers, and that this process is dependent on the disruption of MTs and the activation of Rho kinase (ROCK) and p38 cascades (16). With the realization that barrier-disruptive signaling events may not be limited to the activation of ROCK and p38, we studied the involvement of protein kinase C (PKC) in response to 2ME.

Ezrin/radixin/moesin (ERM) proteins are well-known PKC substrates, emerging as potential candidates in the regulation of barrier permeability (17–19). Believed to serve as cross-linkers between the actin cytoskeleton and plasma membrane, ERM were also shown to be engaged in cell motility and adhesion. Moreover, their ability to organize and maintain specialized membrane domains implied a more diverse function, because these domains define the activation of certain signaling cascades (20).

ERM are characterized by the presence of an N-terminal domain, capable of associating with the membrane, and the C-terminal domain, interacting with F-actin. The function of ERM is conformationally regulated by head-to-tail folding (21), which in turn is controlled by phospholipid binding and phosphorylation (22–25). Numerous kinases were shown to phosphorylate ERM on the conservative threonine residue in the C-terminal domain, including ROCK (24) and PKCs α, β, and θ (17, 26, 27). Other kinases, such

(*Received in original form March 15, 2011; and in final form May 28, 2011*)

This work was supported by American Heart Association grant SDG 0930038N (N.V.B.), National Institutes of Health grants R01 HL-080675 (A.D.V.), R01 HL-083327 (A.D.V.), and R01 HL-067307 (A.D.V.), and a Programmatic Development Award from the Cardiovascular Discovery Institute of Georgia Health Sciences University.

Correspondence and requests for reprints should be addressed to Natalia Bogatcheva, Ph.D., Vascular Biology Center, Georgia Health Sciences University, 1459 Laney Walker Blvd., CB-3701, Augusta, GA 30912. E-mail: nbogatcheva@georgiahealth.edu

This article has an online supplement, which is accessible from this issue's table of contents at www.atsjournals.org

Am J Respir Cell Mol Biol Vol 45. pp 1185–1194, 2011
Originally Published in Press as DOI: 10.1165/rcmb.2011-0092OC on June 9, 2011
Internet address: www.atsjournals.org

as p38 mitogen-activated protein (MAP) kinase (17, 19), were indirectly implicated in the regulation of ERM phosphorylation.

This study tested the hypotheses that ERM proteins are phosphorylated on the regulatory threonine residue in response to 2ME, and are involved in the 2ME-induced barrier dysfunction seen in HPAEC monolayers and murine pulmonary vasculature.

MATERIALS AND METHODS

Materials

2ME was purchased from Sigma (St. Louis, MO). The ROCK inhibitor Y-27632, p38 inhibitor SB203580, and PKC inhibitors Ro-31–7549 and Ro-32–0432 were purchased from Calbiochem (La Jolla, CA). Antibody-recognizing total ERM, phosphorylated ERM (ezrin Thr567, radixin Thr564, and moesin Thr558), phosphorylated PKC isotypes (Thr638/641 for $\alpha\beta\gamma$, and Thr538 for θ), myosin light chains (MLCs), diphosphorylated MLCs, heat shock protein 27 (HSP27), and phosphorylated HSP27 were purchased from Cell Signaling (Beverly, MA). Beta-actin antibody was purchased from Sigma. The glyceraldehyde 3-phosphate dehydrogenase antibody was purchased from Abcam (Cambridge, MA). The V5 antibody, ezrin, radixin, and moesin short interfering RNA (siRNA), and the reagents used for immunofluorescent staining were purchased from Invitrogen (Carlsbad, CA). Nonspecific control siRNA-1 was purchased from Ambion (Austin, TX).

Animal Experiments

Male C57BL/6N mice (weighing 20–25 g) were purchased from Charles River Laboratories (Wilmington, MA). 2ME initially dissolved in DMSO/propylenglycol mixture (1/40, vol/vol) was diluted twice with saline immediately prior to the injection. All injections were administered to the ketamine (150 mg/kg of body weight)/acetopromazine (15 mg/kg)-anesthetized animals. 2ME was administered intravenously via jugular vein in the final volume not exceeding 60 μL. Ro-32–0432 was dissolved in DMSO and diluted 100 times with saline immediately before the injection. We administered 1 mg/kg Ro-32–0432 intravenously in the tail vein, 4 hours before the administration of 2ME. The same dose was readministered together with the dose of 2ME in the jugular vein. Evans blue dye (EBD)–albumin conjugate was administered in the tail vein (30 mg/kg) 1 hour before the animals were killed. All animal studies conformed to National Institutes of Health guidelines. The experimental procedure was approved by the Institutional Animal Care and Use Committee of Georgia Health Sciences University.

Measurement of Lung Permeability

In each anesthetized animal, the chest cavity was opened. For assessment of wet/dry lung weight, lungs were excised without further manipulation, photographed, blotted, weighed, and dried for 24 hours at 65°C. Their weight was documented, and lungs were allowed to dry for another 24 hours, after which the weight was assessed again to assure complete drying of the tissue. For the collection of bronchoalveolar lavage fluid (BALF), lungs were perfused with 1 ml of Hanks' balanced salt solution via the trachea. BALF was centrifuged 15 minutes at 500 × *g*. The concentration of protein in the supernatant was assessed using a BCA Protein Assay Kit (Pierce, Rockford, IL). We washed blood from the same lungs by injecting saline/EDTA via the right ventricle, and collected the lungs for further analysis. The right lung was used for the analysis of proteins, and the left lung was homogenized in formamide to extract EBD (18 hours at 60°C). The homogenate was spun for 30 minutes at 5,000 × *g*. The optical density of supernatants was determined at 620 nm and 750 nm. The concentration of extravasated EBD was calculated using a standard curve, and normalized to lung weight (28).

Cell Culture

HPAECs and human lung microvascular endothelial cells (HLMVECs) were purchased from Lonza (Walkerville, MD), and used at passages 5–7. They were cultured in media containing 5% FBS, and maintained at 37°C in a humidified atmosphere of 5% CO_2/95% air.

The measurement of transendothelial permeability, endothelial cell (EC) imaging, Western immunoblotting, the depletion of endogenous ERM in ECs, the cloning of human endothelial ERM proteins, the transfection of ECs, and statistical analyses are described in the online supplement.

RESULTS

2ME Causes Barrier Dysfunction *In Vitro* and *In Vivo*

Our previous study showed that 2ME was able to evoke increased permeability in HPAEC monolayers, as evidenced by a decrease in transendothelial electrical resistance (TER) and an increase in FITC–dextran flux across the monolayer (16). We compared the effects of 2ME on macrovascular (HPAEC) and microvascular (HLMVEC) endothelia, and show that both types of cell respond to 2ME with MT disintegration, followed by an induction of stress-fiber formation (Figure E1). The assessment of changes in TER and FITC–dextran flux demonstrates that although both macrovascular and microvascular monolayers manifest barrier dysfunction in response to 2ME, the magnitude and duration of HPAEC barrier compromise are higher than those of HMLVECs (Figure E2). This makes the HPAEC a more suitable model for studying mechanisms of 2ME-induced endothelial hyperpermeability.

We also showed that the 2ME-induced decrease in TER can be detected in HPAEC monolayers, both in the absence and presence of serum. In the absence of serum, 5–25 μM 2ME causes a rapid and dramatic drop in TER within the first 10 minutes. Partial barrier restoration is evident within the next hour (Figure 1A). In the presence of serum, higher amounts of 2ME are required to elicit the maximal response (Figure 1B). Monolayers treated with 125 μM 2ME manifest a sustained response, failing to restore their barrier function within 1.5 hours after treatment with 2ME.

We studied the effects of administering intravenous 2ME on lung vascular permeability in mice. We observed that administering a single dose of 2ME caused a significant increase in the extravasation of EBD from the blood lumen to the lung tissue (Figure E3A). The assessment of wet/dry lung weight ratio confirmed that the lungs of mice exposed to 2ME accumulated fluid (Figure E3B), consistent with the manifestation of lung edema. However, the increase of protein level in BALF was insignificant (Figure E3C). The extravasation of EBD was maximal 3 hours after the injection, and subsided to the control level within the next 20 hours (Figure 1C). The injection of different doses of 2ME revealed that the maximal effect on EBD extravasation was achieved at 5 mg/kg (Figure 1D). This dose corresponded to a concentration of approximately 200 μM 2ME in blood.

Effect of 2ME on Barrier Dysfunction Is Attenuated by PKC Inhibitors Ro-31–7549 and Ro-32–0432

We previously showed that the response of HPAECs to 2ME was mediated by the signaling pathways linking MT disruption with the activation of p38 and ROCK cascades (16). Here we examined the involvement of the PKC cascade in 2ME-induced barrier disruption. Figures 2A and 2B show that the PKC inhibitors Ro-31–7549 and Ro-32–0432 were able to attenuate the 2ME-induced decrease in TER, both in the absence and presence of serum. Pretreatment with 10 μM of the inhibitors allowed for an approximately 55% and 45% suppression of the decrease in TER in the absence and presence of serum, respectively.

We next studied the effects of Ro-32–0432 on 2ME-induced vascular leakage *in vivo*. We found that a single administration of Ro-32–0432, 4 hours before injection with 2ME, and followed by a second dose of Ro-32–0432 administered together with the

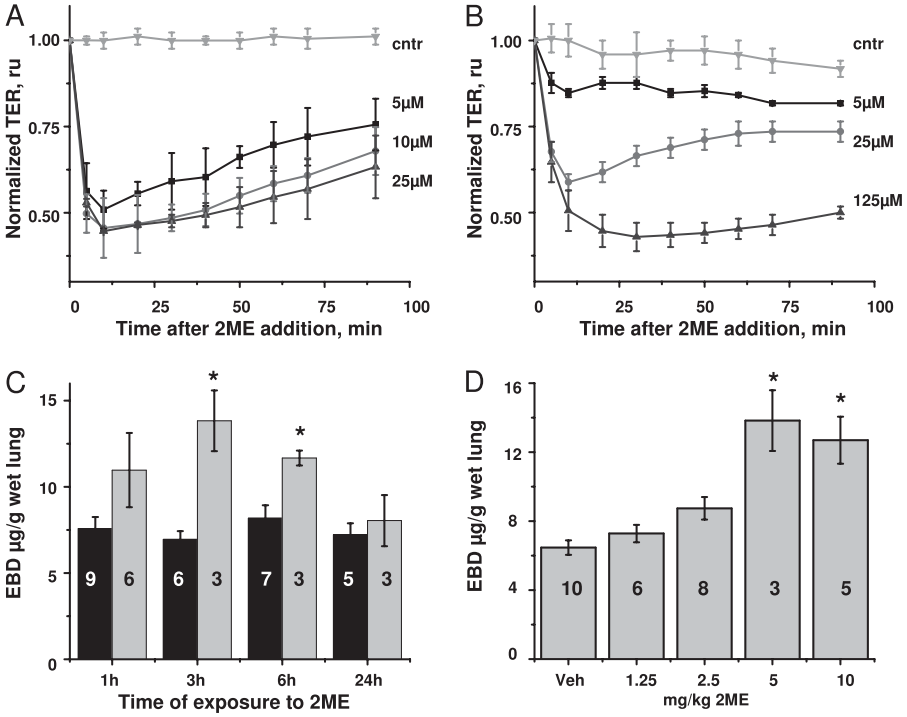

Figure 1. The effect of 2-methoxyestradiol (2ME) on barrier function. (*A* and *B*) Human pulmonary artery endothelial cells (HPAECs) were grown on gold microelectrodes to a resistance of 1,000 Ω. The media were changed to serum-free (*A*) or complete (*B*), 1 hour before stimulation. Monolayers were challenged with vehicle control (cntr; 0.05% DMSO) or indicated concentrations of 2ME. Values for transendothelial electrical resistance (TER) were normalized to the time point of adding 2ME. Values represent the mean ± SEM of three parallel experiments. (*C* and *D*) Male C57BL/6N mice were subjected to intravenous administrations of (*C*) vehicle control (*black columns*) or 5 mg/kg 2ME (*gray columns*) for the times indicated, or (*D*) vehicle control or indicated concentrations of 2ME for 3 hours. The extravasation of Evans blue dye (EBD) in lung tissue was assessed as described in MATERIALS AND METHODS. Values represent the mean ± SEM, with numbers of animals indicated in the figure. $^*P < 0.05$, compared with corresponding control samples. Ru, relative units.

dose of 2ME, significantly attenuated the 2ME-induced extravasation of EBD into lung tissue (Figure 2C). The administration of Ro-32–0432 in the absence of 2ME was accompanied by a nonsignificant increase in vascular leakage. This increase was consistent with the increase in basal permeability seen in response to high concentrations of Ro-32–432 *in vitro* (20 μM; data not shown).

Using phospho-specific anti-PKC antibodies, we showed that exposure to 2ME led to a marked increase in the phosphorylation of the PKCs αβγ and θ (Figure 2D). These data confirmed that PKC is activated in the endothelium in response to 2ME, and demonstrated that the activation of PKC is not limited to classic PKC isotypes. We then studied the effects of PKC inhibitors on the status of PKC αβγ and θ phosphorylation.

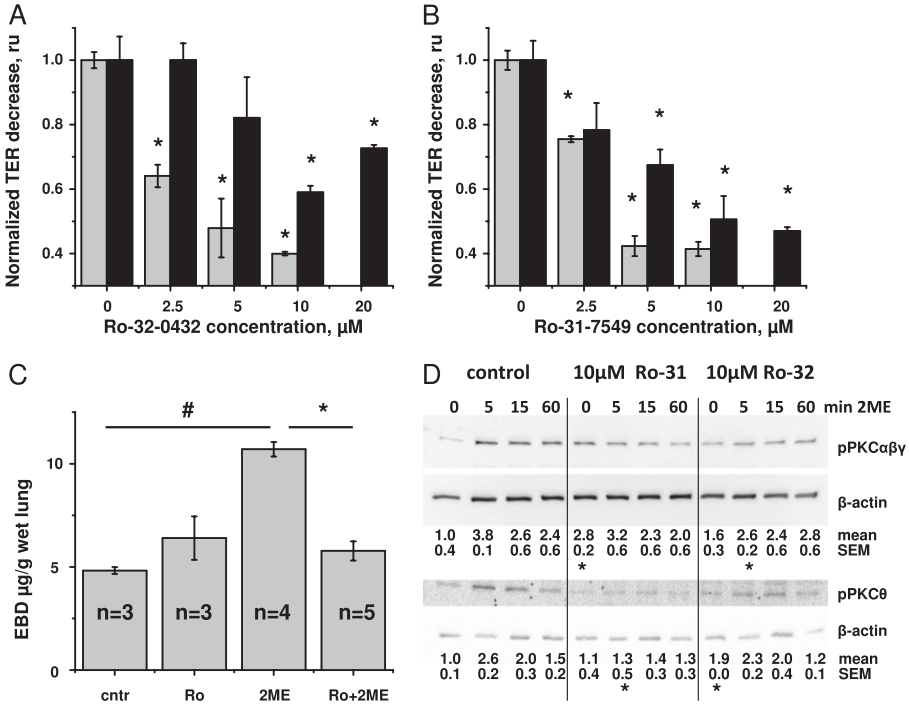

Figure 2. The effect of protein kinase C (PKC) inhibitors Ro-32–0432 and Ro-31–7549 on 2ME-induced barrier dysfunction. (*A* and *B*) HPAECs were grown on gold microelectrodes to the resistance of 1,000 Ω. Media were changed to serum-free (*gray bars*) or complete (*black bars*), 1 hour before stimulation. Monolayers were pretreated with the vehicle control (0 μM inhibitor) or indicated concentration of Ro-32–0432 (*A*) and Ro-31–7549 (*B*) for 15 minutes, and then challenged with 10 μM 2ME. Values of TER were normalized to the time point of adding 2ME. The maximal response to 2ME was assessed and presented as fold response in the absence of inhibitor. (*C*) Male C57BL/6N mice were subjected to an intravenous administration of 1 mg/kg Ro-32–0432 or the corresponding vehicle, and then challenged with 10 mg/kg 2ME or vehicle for 3 hours. The extravasation of EBD in lung tissue was assessed as described in MATERIALS AND METHODS. (*A–C*) Values represent the mean ± SEM from parallel experiments ($n = 3$ for *A* and *B*). $^*P < 0.05$, compared with corresponding pretreatment vehicle control (no inhibitor). $^{\#}P < 0.05$, compared with corresponding treatment control (no 2ME). (*D*) Western blot analysis of cell lysates from HPAEC monolayers, pretreated with vehicle control, 10 μM Ro-31–7549, or 10 μM Ro-32–0432 for 15 min, and then treated with 10 μM 2ME for the times indicated. After transfer, membranes were probed with phospho (p)–PKCαβγ–specific, phospho-PKCθ–specific, and β-actin–specific antibodies. Representative blots of three parallel experiments are depicted. Normalized intensities of phospho-PKCαβγ and phospho-PKCθ are presented as mean ± SEM.

Surprisingly, the application of PKC inhibitor Ro-31–7549 resulted in an increase of basal phosphorylation (seen in the absence of 2ME) for PKC αβγ. The application of Ro-32–0432 resulted in an increase of basal phosphorylation for PKC θ. Importantly, compared with corresponding control samples in the absence of 2ME, the 2ME-induced increase in PKC αβγ and θ phosphorylation was markedly suppressed by pretreatment with Ro-31–7549 and Ro-32–0432 (Figure E4), consistent with the reported specificity of these inhibitors toward classic and novel PKC isotypes (29).

2ME Induces the Phosphorylation of ERM *In Vitro* and *In Vivo*

Because PKCs α, β, and θ were previously implicated in the phosphorylation of ERM (17, 26, 27), we analyzed whether ERM proteins are phosphorylated in response to 2ME. The Western blot analysis of HPAEC monolayers showed that 2ME induced a time-dependent increase in the concentration of phospho-ERM. The maximal phospho-ERM signal was seen 5–15 minutes after the application of 2ME. This signal subsided to control level 60 minutes after the initial challenge (Figure 3A). Comparing the time course of the 2ME-induced drop in TER (Figure 1A) to the time course of ERM phosphorylation (Figure 3A) showed that an increase in ERM phosphorylation correlated with the onset of 2ME-induced hyperpermeability. The analysis of lung extracts from 2ME-treated mice showed that the concentration of phospho-ERM markedly increased in response to 2ME *in vivo* (Figure 3B). Here, again, the increase in phospho-ERM concentration was seen 3 hours after exposure to 2ME, and subsided 24 hours later, coinciding with the increase and decrease of lung permeability in response to 2ME (Figure 1C).

To ascertain that the phosphorylation of ERM is a result of the chain of events initiated by 2ME-induced MT disruption, we pretreated HPAEC monolayers with the MT stabilizer taxol. Pretreatment with taxol diminished the ability of 2ME to induce an increase in ERM phosphorylation (Figure 3C), suggesting that MT disruption is a starting point in the signaling response leading to the phosphorylation of ERM.

We next assessed whether the 2ME-induced phosphorylation of ERM is attenuated by the PKC inhibitors Ro-31–7549 and Ro-32–0432. We observed that both Ro-31–7549 and Ro-32–0432 effectively suppressed the 2ME-induced increase in phospho-ERM concentration (Figures 4A and 4B, and Figure E5), suggesting that this increase is PKC-dependent. Because ERM are also known to constitute a substrate for ROCK-dependent phosphorylation, and ROCK was shown to be activated in response to 2ME (16), we studied how the inhibition of ROCK affects the phosphorylation of ERM in HPAEC monolayers. We showed that pretreatment with Y-27632 did not exert a significant effect on the phosphorylation of ERM. At the same time, the phosphorylation of MLC, subject to regulation via the ROCK/MYPT/PPase1–dependent pathway, was significantly reduced in the presence of Y-27632 (Figure 4A and Figure E5). We also analyzed how the inhibition of p38 affected the 2ME-induced phosphorylation of ERM, and showed that the p38 inhibitor SB203580 attenuated an increase in the phospho-ERM signal (Figure 4B and Figure E5). The effect of SB203580 was also evident in the phosphorylation of HSP27, a downstream substrate of the p38/MAP kinase-activated protein kinase-2 cascade.

Because both PKC and p38 inhibitors affected the phosphorylation of ERM, we assessed the possibility of cross-regulation between PKC and p38-dependent pathways. First, we examined the effects of inhibiting PKC on the phosphorylation of p38 in 2ME-treated cells. The pretreatment of HPAEC monolayers with the PKC inhibitors Ro-31–7549 (Figure 4C) and Ro-32–0432 (data not shown) resulted in a significant increase in the concentration of phospho-p38, both in the absence and presence of 2ME. These data suggest that the attenuation of ERM phosphorylation by Ro-31–7549 and Ro-32–0432 (Figures 4A and 4B) cannot be attributed to the subsequent inactivation of p38, because p38 was overactivated by PKC inhibitors. Next, we examined the effects of inhibiting p38 on the phosphorylation of PKC in 2ME-treated cells. The pretreatment of HPAEC monolayers with the p38 inhibitor SB203580 significantly reduced the 2ME-dependent phosphorylation of PKCs θ (Figure 4D) and αβγ (data not shown). These data indicate that the attenuation of ERM phosphorylation by SB203580 (Figure 4B) can be attributed to the inactivation of PKC, suggesting that the activation of PKC in 2ME-challenged cells is p38-dependent.

Phosphorylation Affects the Localization of ERM in HPAECs

To advance our understanding of the involvement of ERM in response to 2ME, we examined the distribution of ERM and the phospho-ERM signal with an immunofluorescent approach.

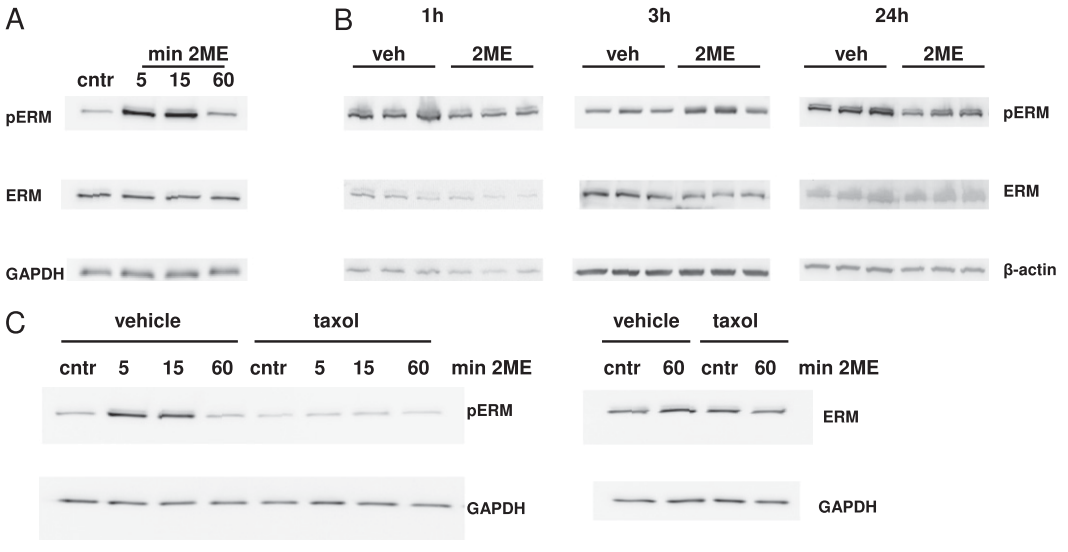

Figure 3. The effect of 2ME on the phosphorylation of ERM. (*A*) Western blot analysis of cell lysates from monolayers, pretreated with vehicle (veh) control (0.05% DMSO) or 10 μM 2ME for the times indicated. A blot representative of three parallel experiments is depicted. (*B*) Western blot analysis of lung lysates from animals injected with vehicle control ($n = 3$) or 5 mg/kg 2ME ($n = 3$) for 1, 3, and 24 hours. (*C*) Western blot analysis of cell lysates from monolayers, pretreated with vehicle control (0.05% DMSO) or 10 μM taxol for 15 minutes and then challenged with 10 μM 2ME for the times indicated. After transfer, membranes were probed with phospho-ERM–specific, ERM-specific (*A*–*C*), glyceraldehyde 3-phosphate dehydrogenase (GAPDH)–specific (*A* and *C*), and β-actin–specific (*B*) antibodies.

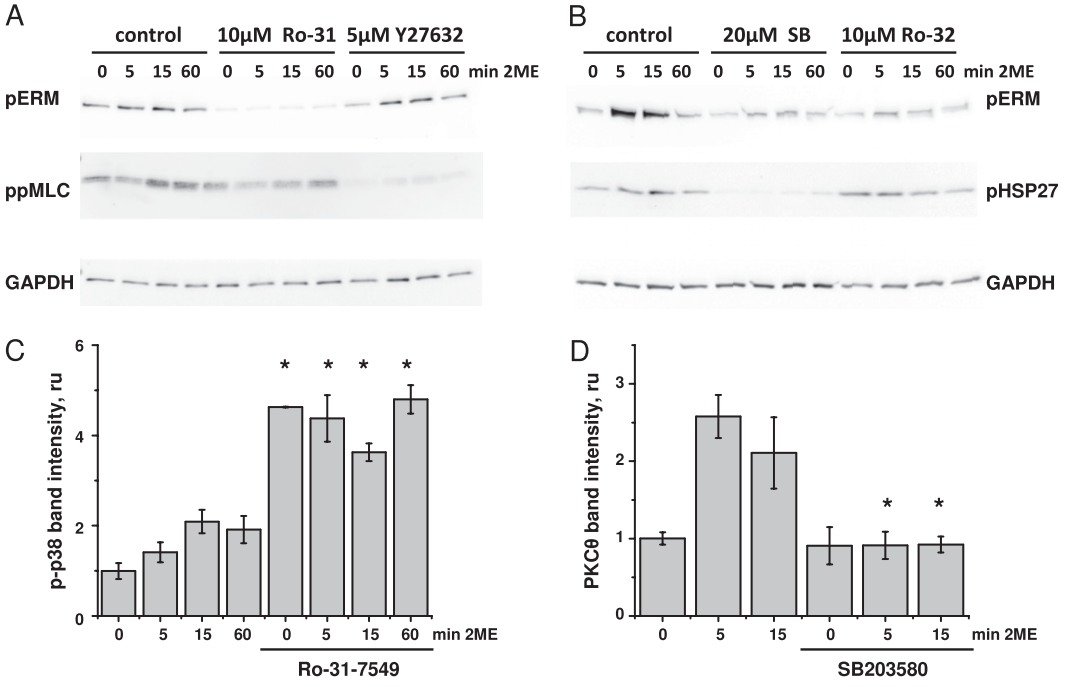

Figure 4. The effects of PKC, Rho kinase (ROCK), and p38 inhibitors on the 2ME-induced phosphorylation of ERM. HPAECs were grown in 12-well plates and pretreated with vehicle control, 10 μM Ro-31–7549, 10 μM Ro-32–0432, 5 μM Y-27632, or 20 μM SB203580 for 15 minutes, and then challenged with vehicle control (0 minutes) or 10 μM 2ME for the times indicated. MLC, myosin light chain; HSP27, heat shock protein 27. (*A* and *B*) After transfer, membranes were probed with phospho-ERM–specific (*A* and *B*), diphospho-MLC–specific (*A*), phospho-HSP27–specific (*B*), and GAPDH-specific (*A* and *B*) antibodies. Blots are representative of three parallel experiments. (*C* and *D*) After transfer, membranes were probed with phospho-p38–specific (*C*), phospho-PKCθ–specific (*D*), and β-actin–specific (*C* and *D*) antibodies. Histograms depict normalized intensities (mean ± SEM, $n = 3$) of phospho-p38 bands (*C*) or phospho-PKCθ bands (*D*). *$P < 0.05$, compared with corresponding pretreatment vehicle control.

In quiescent HPAECs, the ERM signal was visible on the cell periphery, where it colocalized with the cortical actin structures (Figure 5, *left*, and Figure E6, *left*). In stimulated cells, ERM staining mostly coincided with newly formed stress fibers, although the intensity of the ERM signal did not always follow the intensity of F-actin staining (Figure 5, *left*, compare the structures indicated by *arrows* with *asterisks*). The latter fact suggested that some F-actin structures contained higher amounts of ERM, whereas others were ERM-deficient. In contrast to ERM staining, phospho-ERM staining was almost undetectable in quiescent monolayers. In certain areas of quiescent monolayers, a phospho-ERM signal was detected in the spike-like structures overlapping cell–cell contact areas (Figure 5, *right*, *arrow 1*). Treatment with 2ME induced an increase in the amount of phospho-ERM signal, consistent with immunoblotting studies. In cells stimulated with 2ME, the distribution of phospho-ERM was drastically different from that of total ERM. In contracting HPAECs (15 minutes after the initial challenge), the phospho-ERM signal not only did not colocalize with stress fibers, but rather populated the peripheral cytoplasmic areas devoid of F-actin structures (Figure 5, *right*, *arrow 2*). During the partial restoration phase (60 minutes after the initial challenge), a phospho-ERM signal was evident in several structures: spike-like structures originally seen in quiescent cells (Figure 5, *right*, *arrow 1*), peripheral cytoplasmic areas seen during the early response (Figure 5, *right*, *arrow 2*), and bright clusters colocalized with the F-actin branching points (Figure 5, *right*, *arrow 3*). Different localizations of ERM and phospho-ERM proteins suggest that

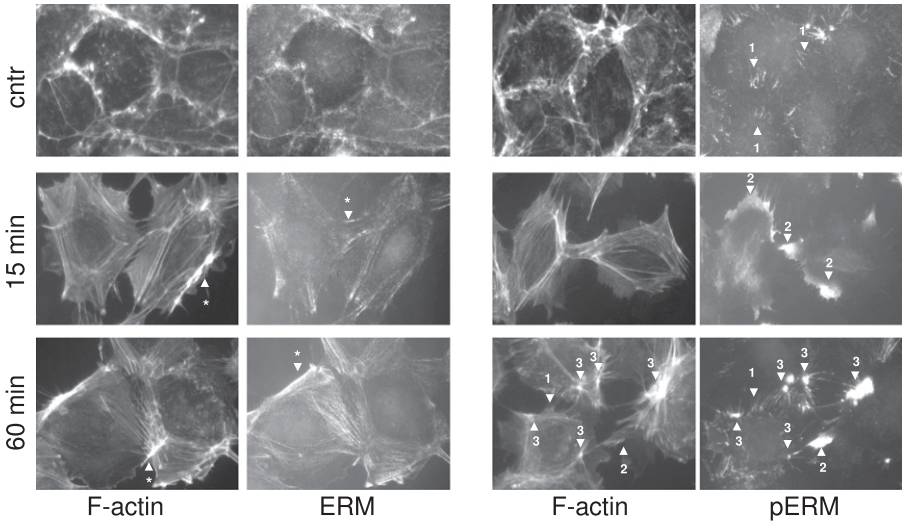

Figure 5. The effects of 2ME on the localization of ERM and phospho-ERM in HPAECs. Cells grown on glass coverslips were pretreated with vehicle control or 10 μM 2ME for the times indicated, fixed, and double-stained with anti-ERM antibody and Alexa594–phalloidin (*left*), or with anti–phospho-ERM antibody and Alexa594–phalloidin (*right*). 2ME induces the formation of stress fibers in HPAECs. The ERM signal colocalizes with cortical actin structures in quiescent cells and stress fibers in 2ME-challenged cells, although some F-actin structures display preferential or deficient staining with ERM antibodies (*left*, *arrows* with *asterisks*). The phospho-ERM signal, almost undetectable in quiescent monolayers, is evident only in peripheral spike-like structures overlapping cell–cell borders (*right*, *arrow 1*). Within 15 minutes of applying 2ME, the phospho-ERM signal is detected in peripheral areas, where it does not colocalize with F-actin structures (*arrow 2*). One hour after applying 2ME, a phospho-ERM signal is detectable in the spike-like structures characteristic of quiescent cells (*arrow 1*), in peripheral areas devoid of F-actin (*arrow 2*), and in clusters colocalizing with areas of intense F-actin staining (*arrow 3*). Merged images (ERM/F-actin and phospho-ERM/F-actin) are presented in Figure E6.

phosphorylation changes the properties and function of ERM. Changes in the localization of phospho-ERM during the phase of active contraction (15 minutes of treatment with 2ME) and the phase of partial barrier restoration (60 minutes of treatment) indicate that phospho-ERM may be involved in both processes.

Knockdown of ERM Suppresses 2ME-Induced Barrier Hyperpermeability

To evaluate the role of individual ERM proteins in 2ME-induced barrier dysfunction, we used siRNAs targeting ezrin, radixin, and moesin mRNA. Pretreatment with specific siRNAs inhibited the expression of corresponding proteins, without affecting the expression of other ERM proteins (Figure 6A). In HPAECs, ezrin, radixin, and moesin appear as bands of similar molecular weight. Using anti-ERM antibody raised against the peptide surrounding Thr567 of human ezrin (conservative within ERM), we showed that total ERM expression was significantly affected by pretreatment with moesin siRNA only, suggesting that moesin is the major ERM in HPAECs.

The analysis of the effect of individual knockdowns on the resistance of quiescent monolayers revealed that the depletion of individual ERM proteins does not significantly affect basal permeability (Figure 6B). On the contrary, the 2ME-induced drop in TER was markedly alleviated by the depletion of ezrin, radixin, or moesin (Figure 6C). Interestingly, although the depletion of radixin alleviated the early phase of 2ME-induced barrier dysfunction without affecting the late phase, the depletion of ezrin and moesin augmented the barrier during early and late responses to 2ME. The effect of moesin depletion superseded the effects of ezrin and radixin depletion during the late phase of response to 2ME.

The Phosphorylation of ERM Is Critical for 2ME-Induced Barrier Dysfunction

Because our previous data showed that ERM and phospho-ERM are likely to have distinct functions during the response to 2ME, we asked whether the effect of ERM depletion on the response of 2ME is mediated by a deficit of total ERM or phospho-ERM. To answer this question, we assessed whether the alleviating effect of PKC inhibitors on 2ME-induced barrier dysfunction would still be evident in the absence of ERM. Nonsilencing RNA (NS)–pretreated cells responded to 2ME with a rapid loss of transendothelial resistance, which was partially restored within the next hour (Figure 7A). Ro-31–7549 pretreatment of these monolayers significantly attenuated the effect of 2ME. This attenuation reached 52% at maximum, and was clearly seen until 40 minutes after the addition of 2ME. HPAEC monolayers pretreated with a mixture of ezrin, radixin, and moesin siRNAs responded to 2ME with a decrease in TER of a significantly lower magnitude than that of NS-pretreated cells. When ERM-depleted monolayers were pretreated with Ro-31–7549, the attenuation of the 2ME-induced decrease in TER reached 37% at maximum, and was evident for only a short period of time (first 15 minutes of response). These data clearly show that both the depletion of ERM and inhibition of PKC protect HPAEC monolayers from 2ME-induced barrier dysfunction. They also show that in the absence of ERM, the alleviating effect of PKC inhibition on 2ME-induced barrier dysfunction is less pronounced.

To substantiate the causative role of ERM phosphorylation in 2ME-induced barrier disruption, we compared the effects of the PKC inhibitor on the 2ME-induced response of HPAECs overexpressing the phosphorylation-deficient mutants of ezrin (Thr567Ala), radixin (Thr564Ala), and moesin (Thr558Ala). Western blot analysis confirmed that cells transfected with wild-type or mutant ERM proteins expressed detectable concentrations of these proteins 48 hours after nucleofection (Figure 7C). The analysis of ERM phosphorylation showed that monolayers overexpressing mutant ERM displayed less of an increase in phospho-ERM concentrations than did monolayers overexpressing wild-type ERM (Figure 7D). Because nucleofected monolayers (including those subjected to sham nucleofection) were slow to form contacts and were vulnerable to changes of medium, we performed our experiments in the presence of serum. Wild-type ERM-expressing monolayers responded to 2ME with a significant decrease in TER. This decrease was attenuated by pretreatment with Ro-31–7549 (Figure 7B). Attenuation reached 21% at maximum, and was clearly observed

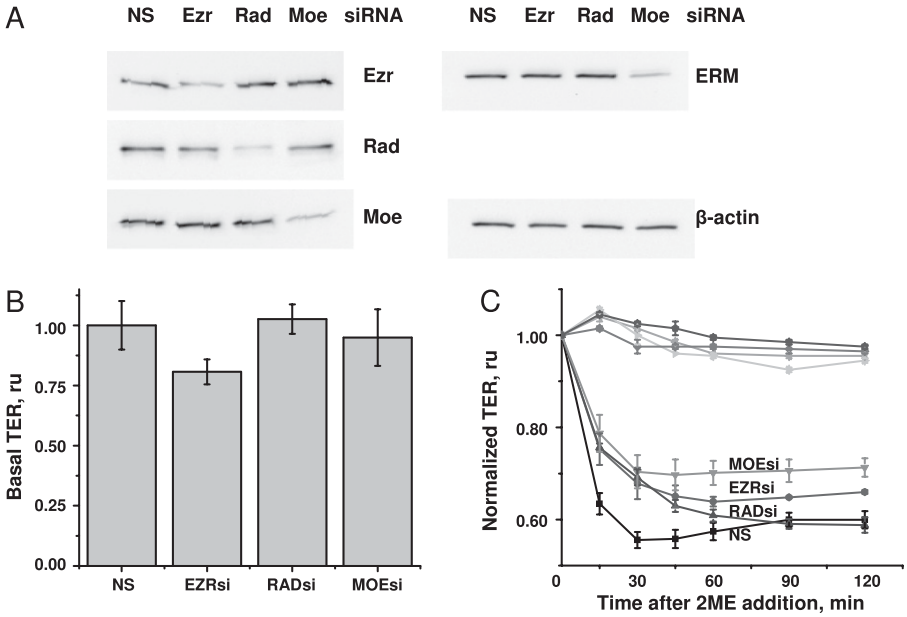

Figure 6. The effect of ERM depletion on the permeability of HPAEC monolayers. Cells grown in 12-well plates or electric cell-substrate impedance sensing (ECIS) chambers were pretreated with 50 nM individual short interfering RNAs (siRNAs) for 48 hours. (*A*) Western blots of cell lysates from monolayers pretreated with nonsilencing (NS), ezrin (Ezr)–specific, radixin (Rad)–specific, and moesin (Moe)–specific siRNAs. After transfer, membranes were probed with ezrin-specific, radixin-specific, moesin-specific, and ERM-specific antibodies. β-actin staining was used as loading control. (*B*) The effect of individual ERM depletions on the basal resistance of HPAECs. The resistance of unchallenged monolayers was analyzed ($n = 4$) and expressed as fold of the resistance of unchallenged cells pretreated with nonsilencing siRNA. ESRsi, ezrin-specific siRNA; RADsi, radixin-specific siRNA ; MOEsi, moesin-specific siRNA. (*C*) The effects of individual ERM depletions on 2ME-induced hyperpermeability. The resistance of siRNA-pretreated monolayers was normalized to the time point of adding 2ME. TER values of vehicle control–treated monolayers (*curves at the top*) and 10 μM 2ME-treated monolayers (*curves at the bottom*) were pooled from three parallel experiments and expressed as mean ± SEM.

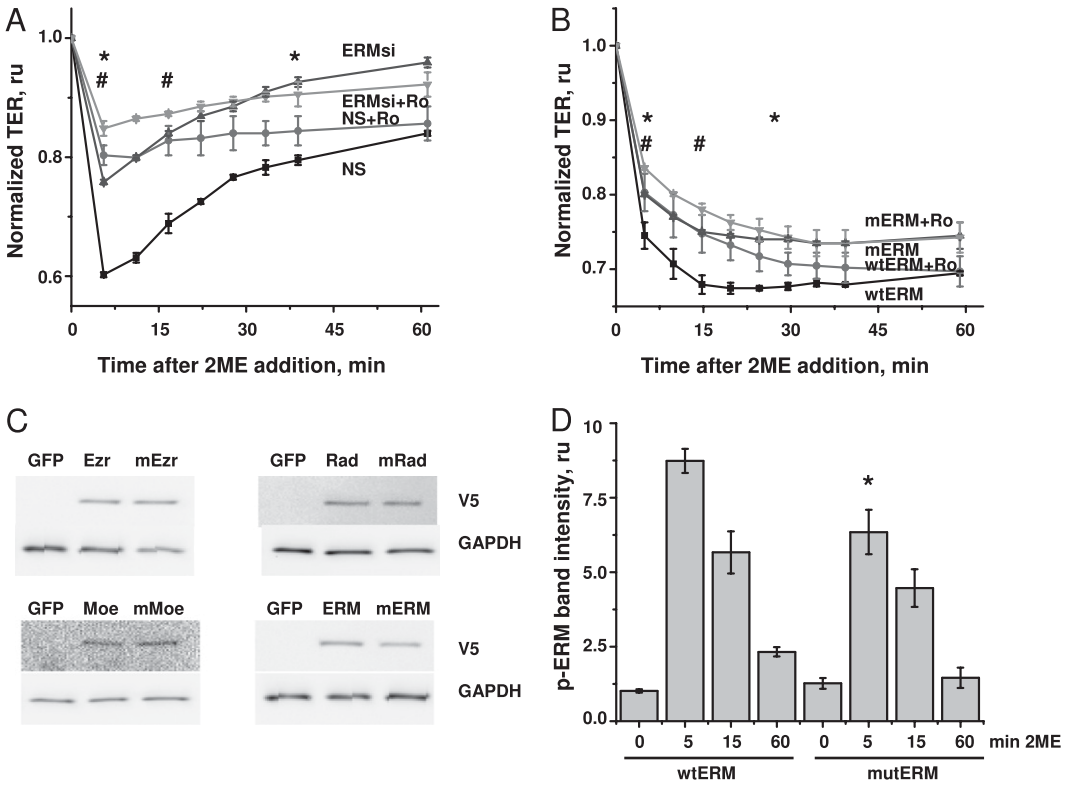

Figure 7. The effect of ERM depletion or the suppression of ERM phosphorylation on Ro-31–7549–mediated alleviation of barrier dysfunction in 2ME-treated HPAECs. (*A*) Cells grown on gold microelectrodes were pretreated with nonsilencing (*squares* and *circles*) RNA or a mixture of ERM-specific siRNAs (ERMsi; *triangles* and *inverse triangles*) for 48 hours. Media were changed to serum-free, 1 hour before the experiment. Cells were then preincubated with 2.5 μM Ro-31–7549 (Ro; *circles* and *inverse triangles*) or vehicle control (*squares* and *triangles*), and challenged with 5 μM 2ME. The resistance of siRNA-pretreated monolayers was normalized to the time point of adding 2ME. Values of TER were pooled from three parallel experiments and expressed as mean ± SEM. Ro-31–7549 attenuated the response to 2ME between time points, as indicated by an asterisk in NS-transfected monolayers, and by a pound sign in ERM siRNA–transfected monolayers. (*B*) Cells were electroporated to introduce a mixture of wild-type (wt) ezrin-expressing, radixin-expressing, and moesin-expressing vectors (*squares* and *circles*), or a mixture of phosphorylation-deficient mutants (m) of these proteins (*triangles* and inverse triangles), and then plated in the ECIS chambers. Forty-eight hours later, the media were changed to fresh and complete, 1 hour before the experiment. Cells were then preincubated with 5 μM Ro-31–7549 (*circles* and *inverse triangles*) or vehicle control (*squares* and *triangles*), and challenged with 25 μM 2ME. The resistance of transfected monolayers was normalized to the time point of adding 2ME. Values of TER were pooled from three parallel experiments and expressed as mean ± SEM. Pretreatment with Ro-31–7549 attenuated the response to 2ME between time points, as indicated by an asterisk in wild-type ERM–transfected monolayers, or by a pound sign in mutant ERM–transfected monolayers. (*C*) Western blots of lysates from HPAECs nucleofected with vectors expressing green fluorescent protein (GFP), ezrin (wild-type and mutant), radixin (wild-type and mutant), and moesin (wild-type and mutant). After transfer, membranes were probed with V5 tag-specific antibodies. GAPDH staining was used as loading control. (*D*) HPAECs were nucleofected with a mixture of wild-type or mutant ERM, and then stimulated with 10 μM 2ME, lysed, and subjected to Western blot analysis. The intensity of phospho-ERM bands was normalized to the intensity of ERM bands, and expressed as fold of control values. Values represent the mean ± SEM of three independent transfections. *$P < 0.05$, compared with corresponding time point of cells expressing wild-type ERM.

during the first 30 minutes of response. Mutant ERM-expressing monolayers responded to 2ME with a decrease in TER of lower magnitude than in wild-type ERM-expressing cells. The attenuation of the decrease in 2ME via Ro-31–7549 reached 13% at maximum, and was only significant during the first 15 minutes of response. In accordance with the results in Figure 7A, these data show that the alleviating effect of PKC inhibition was less pronounced in cells expressing phosphorylation-deficient forms of ERM.

DISCUSSION

We previously showed that the MT-disrupting agent 2ME causes EC monolayer hyperpermeability for ions and macromolecular tracers (16). Here we show that 2ME induces endothelial barrier dysfunction *in vivo*, as made apparent by the increased extravasation of EBD and water from the murine vascular lumen to pulmonary tissue. Similar to H_2O_2 and histamine, which disrupt the endothelial barrier within minutes of initial challenge *in vitro* (30, 31) but require longer exposures to induce detectable vascular leakage *in vivo* (32–34), 2ME-induced changes in vascular permeability reach a significant level only 3 hours after the addition of 2ME (Figure 1). Our data confirm the previously shown barrier-disruptive effect of 2ME (16), and provide a physiological explanation for the vascular-related side effects manifested in clinical trials of 2ME (2–6).

We previously showed that 2ME-induced barrier compromise depends on the activation of p38 and ROCK pathways (16). Here we showed (for the first time, to the best of our knowledge) that the PKC pathway is also activated in response to 2ME, and this activation contributes to the loss of barrier function, because PKC inhibitors alleviate 2ME-induced vascular permeability *in vitro* and *in vivo*. Whereas the involvement of PKC in barrier dysfunction induced by different edemagenic agents is well-documented (35, 36), the data regarding the activation of PKC in response to MT disruption are novel, and extend our understanding of the mechanisms linking cytoskeletal rearrangement to downstream signaling pathways.

Because ERM proteins are known substrates for PKC (17, 26, 27, 37), this study next examined the process of ERM phosphorylation in response to 2ME. Our results demonstrated that ERM were readily phosphorylated in 2ME-treated HPAEC monolayers and lung tissue, and an increase in the phosphorylation of ERM was driven by MT disruption as a primary event. We found that the phosphorylation of ERM in HPAECs depended on the activity of PKC and p38, but was not regulated

in a ROCK-dependent manner. Our results were different from those in previous studies (19) showing that the phosphorylation of ERM was ROCK-dependent in response to advanced glycation end products. Altogether, these observations suggest that upstream pathways leading to the phosphorylation of ERM can vary from endothelium to endothelium or from stimuli to stimuli.

Although the site of ERM phosphorylation does not contain the consensus sequence recognized by p38 kinase, ERM can be phosphorylated by some downstream kinases of the p38-dependent cascade. To assess whether PKC-dependent and p38-dependent increases in the phosphorylation of ERM are two independent events, or one kinase lies upstream of another, we assessed whether the activity of p38 is regulated by PKC in 2ME-challenged cells. We discovered that PKC inhibitors do not inhibit p38, but rather cause the hyperactivation of p38. These data suggest that the activation of PKC is not likely to lie upstream of the p38 cascade in 2ME-challenged cells. We next asked whether the activity of PKC is regulated by p38 in response to 2ME. We found that the phosphorylation of both classic and novel isotypes of PKC is attenuated by p38 inhibition, suggesting that the phosphorylation of ERM in response to 2ME occurs in a p38→PKC–dependent manner. However, the colocalization of PKCs α and β with MTs, as seen in certain types of cells (38, 39) allowed us to speculate that, to some extent, the activation of classical PKC isoforms may be a direct result of MT disruption, and therefore can be achieved independently of the p38 activation process.

The experiments demonstrating that ERM are phosphorylated in response to 2ME prompted us to examine the role of ERM in 2ME-induced cytoskeletal changes. In quiescent cells, ERM proteins were shown to be present in the cytoplasm in inactive form, whereas the phosphorylation of a conservative threonine residue near the C-terminus enabled them to interact with both the cytoskeleton and membrane (37). However, in some cells, an association of ezrin or radixin with the actin cytoskeleton or cell membrane was evident in the absence of stimuli (40, 41). We found that in quiescent HPAECs, the ERM signal colocalizes with cortical actin, whereas the phospho-ERM signal is very low and can only be detected in certain monolayer areas with spike-like structures present on the cell borders. In 2ME-challenged cells, the intracellular localization of ERM significantly differed from the localization of phospho-ERM, suggesting that only a minor fraction of ERM is phosphorylated. Our data were consistent with previous reports (17, 18) showing that phospho-ERM were mostly localized to the peripheral area in endothelial cells undergoing contraction and a loss of monolayer integrity. Of interest, the colocalization of phospho-ERM with F-actin branching points was also described in endothelial cells (42). These branching points were enriched with signaling molecules such as PKCα/β_{II}, suggesting an integration of mechanical and soluble signals at these locales. The presence of phospho-ERM/F-actin–enriched microstructures in the cells undergoing the late phase of response to 2ME led us to hypothesize that phospho-ERM act to reorganize the endothelial cytoskeleton, during both the onset of barrier compromise and the phase of partial barrier restoration.

We next examined the role of ERM in 2ME-induced hyperpermeability by depleting these proteins, using a siRNA approach. Ezrin, radixin, and moesin siRNAs were efficient and specific in inhibiting the expression of their presumed targets. The depletion of any of the three ERM proteins attenuated the increase in 2ME-induced permeability. These data clearly suggest that ERM proteins are critically involved in the development of 2ME-induced endothelial permeability.

Because we show here that ERM colocalize with F-actin structures in quiescent and 2ME-challenged cells, we next asked if the effect of ERM depletion on barrier dysfunction was dependent on the reduction of ERM phosphorylation or on an ablation of the association of ERM with the cytoskeleton. Insofar as ERM proteins are not the sole substrates for PKC, we were also interested in determining the extent of Ro-31–7549–dependent alleviation of barrier dysfunction in the absence of ERM. Using triple ERM siRNA knockdown, we tested the effect of Ro-31–7549 on 2ME-induced hyperpermeability, and found that the effect of Ro-31–7549 was less pronounced in ERM-depleted monolayers. We extended these studies using unphosphorylatable ERM constructs, and confirmed that the Ro-31–7549–mediated alleviation of barrier dysfunction was less sustained when the unphosphorylatable form of ERM was present. These data corroborated the critical role of ERM phosphohorylation in the development of 2ME-induced barrier compromise.

The underlying mechanism through which ERM proteins regulate 2ME-induced cytoskeletal changes and permeability remains to be determined. ERM proteins are known to promote the *de novo* assembly of F-actin (43), to interact with and activate focal adhesion kinase (44), and to activate Rho signaling via the Rho guanosine diphosphate dissociation inhibitor (Rho GDI) (45). The latter fact is of specific interest for our future studies, because Rho signaling is known to be activated in 2ME-challenged cells, and critically involved in the development of 2ME-induced barrier dysfunction (16). So far, the interaction of ERM with Rho GDI was only shown to be dependent on the phosphorylation of Thr235 (N-terminal ERM domain) by cyclin-dependent kinase 5 (46). Future studies will be needed to show whether the PKC-dependent phosphorylation of ERM at the C-terminal site regulates this interaction. If that is the case, the MT disruption–dependent activation of PKC with the consequent phospho-ERM–dependent inactivation of Rho GDI may represent yet another pathway by which MT rearrangement is linked to the formation of stress fibers and endothelial contraction.

In conclusion, the present study demonstrates that in endothelial cells, 2ME evokes a complex signaling response that includes the activation of PKC and the phosphorylation of ERM proteins. The phosphorylation of ERM, occurring in a p38/PKC–dependent manner, changes the localization of ERM. ERM proteins are critically involved in the barrier-disruptive response induced in the endothelium by 2ME. This study extends previous knowledge about the involvement of PKC and ERM in endothelial barrier regulation, and also characterizes an additional mechanism of 2ME-induced barrier dysfunction.

Author Disclosure: None of the authors has a financial relationship with a commercial entity that has an interest in the subject of this manuscript.

Acknowledgments: The authors are grateful to Drs. D. Fulton and S. Black from Georgia Health Sciences University for help with the preparation of ERM mutants. The authors thank Ms. Nurgul Moldobaeva and Dr. Bolot Mambetsariev for technical assistance with some of the experiments. The authors are grateful to Ms. Jenna Gallops for help with preparation of the manuscript.

References

1. Sutherland TE, Anderson RL, Hughes RA, Altmann E, Schuliga M, Ziogas J, Stewart AG. 2-methoxyestradiol: a unique blend of activities generating a new class of anti-tumour/anti-inflammatory agents. *Drug Discov Today* 2007;12:577–584.
2. Sweeney C, Liu G, Yiannoutsos C, Kolesar J, Horvath D, Staab MJ, Fife K, Armstrong V, Treston A, Sidor C, *et al*. A Phase II multicenter, randomized, double-blind, safety trial assessing the pharmacokinetics, pharmacodynamics, and efficacy of oral 2-methoxyestradiol capsules in hormone-refractory prostate cancer. *Clin Cancer Res* 2005;11:6625–6633.
3. Dahut WL, Lakhani NJ, Gulley JL, Arlen PM, Kohn EC, Kotz H, McNally D, Parr A, Nguyen D, Yang SX, *et al*. Phase I clinical trial of

oral 2-methoxyestradiol, an antiangiogenic and apoptotic agent, in patients with solid tumors. *Cancer Biol Ther* 2006;5:22–27.
4. James J, Murry DJ, Treston AM, Storniolo AM, Sledge GW, Sidor C, Miller KD. Phase I safety, pharmacokinetic and pharmacodynamic studies of 2-methoxyestradiol alone or in combination with docetaxel in patients with locally recurrent or metastatic breast cancer. *Invest New Drugs* 2007;25:41–48.
5. Rajkumar SV, Richardson PG, Lacy MQ, Dispenzieri A, Greipp PR, Witzig TE, Schlossman R, Sidor CF, Anderson KC, Gertz MA. Novel therapy with 2-methoxyestradiol for the treatment of relapsed and plateau phase multiple myeloma. *Clin Cancer Res* 2007;13:6162–6167.
6. Matei D, Schilder J, Sutton G, Perkins S, Breen T, Quon C, Sidor C. Activity of 2 methoxyestradiol (panzem NCD) in advanced, platinum-resistant ovarian cancer and primary peritoneal carcinomatosis: a Hoosier Oncology Group trial. *Gynecol Oncol* 2009;115: 90–96.
7. Tevaarwerk AJ, Holen KD, Alberti DB, Sidor C, Arnott J, Quon C, Wilding G, Liu G. Phase I trial of 2-methoxyestradiol nanocrystal dispersion in advanced solid malignancies. *Clin Cancer Res* 2009;15: 1460–1465.
8. Foster PA, Ho YT, Newman SP, Leese MP, Potter BV, Reed MJ, Purohit A. STX140 and STX641 cause apoptosis via the intrinsic mitochondrial pathway and down-regulate survivin and XIAP expression in ovarian and prostate cancer cells. *Anticancer Res* 2009;29: 3751–3757.
9. Newman SP, Foster PA, Ho YT, Day JM, Raobaikady B, Kasprzyk PG, Leese MP, Potter BV, Reed MJ, Purohit A. The therapeutic potential of a series of orally bioavailable anti-angiogenic microtubule disruptors as therapy for hormone-independent prostate and breast cancers. *Br J Cancer* 2007;97:1673–1682.
10. Newman SP, Foster PA, Stengel C, Day JM, Ho YT, Judde JG, Lassalle M, Prevost G, Leese MP, Potter BV, *et al*. STX140 is efficacious *in vitro* and *in vivo* in taxane-resistant breast carcinoma cells. *Clin Cancer Res* 2008;14:597–606.
11. Parsons MF, Foster PA, Chander SK, Jhalli R, Newman SP, Leese MP, Potter BV, Purohit A, Reed MJ. The *in vivo* properties of STX243: a potent angiogenesis inhibitor in breast cancer. *Br J Cancer* 2008;99: 1433–1441.
12. D'Amato RJ, Lin CM, Flynn E, Folkman J, Hamel E. 2-methoxyestradiol, an endogenous mammalian metabolite, inhibits tubulin polymerization by interacting at the colchicine site. *Proc Natl Acad Sci USA* 1994;91: 3964–3968.
13. Birukova AA, Birukov KG, Gorshkov B, Liu F, Garcia JG, Verin AD. MAP kinases in lung endothelial permeability induced by microtubule disassembly. *Am J Physiol Lung Cell Mol Physiol* 2005;289:L75–L84.
14. Birukova AA, Smurova K, Birukov KG, Usatyuk P, Liu F, Kaibuchi K, Ricks-Cord A, Natarajan V, Alieva I, Garcia JG, *et al*. Microtubule disassembly induces cytoskeletal remodeling and lung vascular barrier dysfunction: role of Rho-dependent mechanisms. *J Cell Physiol* 2004; 201:55–70.
15. Verin AD, Birukova A, Wang P, Liu F, Becker P, Birukov K, Garcia JG. Microtubule disassembly increases endothelial cell barrier dysfunction: role of MLC phosphorylation. *Am J Physiol Lung Cell Mol Physiol* 2001;281:L565–L574.
16. Bogatcheva NV, Adyshev D, Mambetsariev B, Moldobaeva N, Verin AD. Involvement of microtubules, p38, and Rho kinases pathway in 2-methoxyestradiol–induced lung vascular barrier dysfunction. *Am J Physiol Lung Cell Mol Physiol* 2007;292:L487–L499.
17. Koss M, Pfeiffer GR II, Wang Y, Thomas ST, Yerukhimovich M, Gaarde WA, Doerschuk CM, Wang Q. Ezrin/radixin/moesin proteins are phosphorylated by TNF-alpha and modulate permeability increases in human pulmonary microvascular endothelial cells. *J Immunol* 2006;176:1218–1227.
18. Csortos C, Czikora I, Bogatcheva NV, Adyshev DM, Poirier C, Olah G, Verin AD. TIMAP is a positive regulator of pulmonary endothelial barrier function. *Am J Physiol Lung Cell Mol Physiol* 2008;295:L440–L450.
19. Guo X, Wang L, Chen B, Li Q, Wang J, Zhao M, Wu W, Zhu P, Huang X, Huang Q. ERM protein moesin is phosphorylated by advanced glycation end products and modulates endothelial permeability. *Am J Physiol Heart Circ Physiol* 2009;297:H238–H246.
20. Fehon RG, McClatchey AI, Bretscher A. Organizing the cell cortex: the role of ERM proteins. *Nat Rev Mol Cell Biol* 2010;11:276–287.
21. Gary R, Bretscher A. Ezrin self-association involves binding of an N-terminal domain to a normally masked C-terminal domain that includes the F-actin binding site. *Mol Biol Cell* 1995;6:1061–1075.
22. Nakamura F, Amieva MR, Furthmayr H. Phosphorylation of threonine 558 in the carboxyl-terminal actin-binding domain of moesin by thrombin activation of human platelets. *J Biol Chem* 1995;270:31377–31385.
23. Yonemura S, Matsui T, Tsukita S. Rho-dependent and -independent activation mechanisms of ezrin/radixin/moesin proteins: an essential role for polyphosphoinositides *in vivo*. *J Cell Sci* 2002;115:2569–2580.
24. Matsui T, Maeda M, Doi Y, Yonemura S, Amano M, Kaibuchi K, Tsukita S. Rho-kinase phosphorylates COOH-terminal threonines of ezrin/radixin/moesin (ERM) proteins and regulates their head-to-tail association. *J Cell Biol* 1998;140:647–657.
25. Fievet BT, Gautreau A, Roy C, Del Maestro L, Mangeat P, Louvard D, Arpin M. Phosphoinositide binding and phosphorylation act sequentially in the activation mechanism of ezrin. *J Cell Biol* 2004;164: 653–659.
26. Ng T, Parsons M, Hughes WE, Monypenny J, Zicha D, Gautreau A, Arpin M, Gschmeissner S, Verveer PJ, Bastiaens PI, *et al*. Ezrin is a downstream effector of trafficking PKC–integrin complexes involved in the control of cell motility. *EMBO J* 2001;20:2723–2741.
27. Pietromonaco SF, Simons PC, Altman A, Elias L. Protein kinase C–theta phosphorylation of moesin in the actin-binding sequence. *J Biol Chem* 1998;273:7594–7603.
28. Moitra J, Sammani S, Garcia JG. Re-evaluation of Evans blue dye as a marker of albumin clearance in murine models of acute lung injury. *Transl Res* 2007;150:253–265.
29. Wilkinson SE, Parker PJ, Nixon JS. Isoenzyme specificity of bisindolylmaleimides, selective inhibitors of protein kinase C. *Biochem J* 1993;294:335–337.
30. Moldobaeva A, Welsh-Servinsky LE, Shimoda LA, Stephens RS, Verin AD, Tuder RM, Pearse DB. Role of protein kinase G in barrier-protective effects of CGMP in human pulmonary artery endothelial cells. *Am J Physiol Lung Cell Mol Physiol* 2006;290:L919–L930.
31. Guo M, Breslin JW, Wu MH, Gottardi CJ, Yuan SY. VE-cadherin and beta-catenin binding dynamics during histamine-induced endothelial hyperpermeability. *Am J Physiol Cell Physiol* 2008;294:C977–C984.
32. Meiring JJ, Borm PJ, Bagate K, Semmler M, Seitz J, Takenaka S, Kreyling WG. The influence of hydrogen peroxide and histamine on lung permeability and translocation of iridium nanoparticles in the isolated perfused rat lung. *Part Fibre Toxicol* 2005;2:3.
33. Walkenstein MD, Peterson BT, Gerber JE, Hyde RW. Histamine-induced pulmonary edema distal to pulmonary arterial occlusion. *J Appl Physiol* 1985;58:1092–1098.
34. Nemmar A, Hamoir J, Nemery B, Gustin P. Evaluation of particle translocation across the alveolo-capillary barrier in isolated perfused rabbit lung model. *Toxicology* 2005;208:105–113.
35. Bogatcheva NV, Verin AD. The role of cytoskeleton in the regulation of vascular endothelial barrier function. *Microvasc Res* 2008;76:202–207.
36. Komarova Y, Malik AB. Regulation of endothelial permeability via paracellular and transcellular transport pathways. *Annu Rev Physiol* 2010;72:463–493.
37. Simons PC, Pietromonaco SF, Reczek D, Bretscher A, Elias L. C-terminal threonine phosphorylation activates ERM proteins to link the cell's cortical lipid bilayer to the cytoskeleton. *Biochem Biophys Res Commun* 1998;253:561–565.
38. Dykes AC, Fultz ME, Norton ML, Wright GL. Microtubule-dependent PKC-alpha localization in A7R5 smooth muscle cells. *Am J Physiol Cell Physiol* 2003;285:C76–C87.
39. Volkov Y, Long A, McGrath S, Ni Eidhin D, Kelleher D. Crucial importance of PKC-beta(I) in LFA-1–mediated locomotion of activated T cells. *Nat Immunol* 2001;2:508–514.
40. Lamb RF, Ozanne BW, Roy C, McGarry L, Stipp C, Mangeat P, Jay DG. Essential functions of ezrin in maintenance of cell shape and lamellipodial extension in normal and transformed fibroblasts. *Curr Biol* 1997;7:682–688.
41. Lopez JP, Turner JR, Philipson LH. Glucose-induced ERM protein activation and translocation regulates insulin secretion. *Am J Physiol Endocrinol Metab* 2010;299:E772–E785.

42. Jensen PV, Larsson LI. Actin microdomains on endothelial cells: association with CD44, ERM proteins, and signaling molecules during quiescence and wound healing. *Histochem Cell Biol* 2004;121:361–369.
43. Defacque H, Egeberg M, Habermann A, Diakonova M, Roy C, Mangeat P, Voelter W, Marriott G, Pfannstiel J, Faulstich H, *et al*. Involvement of ezrin/moesin in *de novo* actin assembly on phagosomal membranes. *EMBO J* 2000;19:199–212.
44. Poullet P, Gautreau A, Kadare G, Girault JA, Louvard D, Arpin M. Ezrin interacts with focal adhesion kinase and induces its activation independently of cell-matrix adhesion. *J Biol Chem* 2001;276:37686–37691.
45. Takahashi K, Sasaki T, Mammoto A, Takaishi K, Kameyama T, Tsukita S, Takai Y. Direct interaction of the Rho GDP dissociation inhibitor with ezrin/radixin/moesin initiates the activation of the Rho small G protein. *J Biol Chem* 1997;272:23371–23375.
46. Yang HS, Hinds PW. Phosphorylation of ezrin by cyclin-dependent kinase 5 induces the release of Rho GDP dissociation inhibitor to inhibit Rac1 activity in senescent cells. *Cancer Res* 2006;66:2708–2715.